Boundary Conditions for Direct Computation of Aerodynamic Sound Generation

T. Colonius, S. K. Lele, P. Moin

Boundary Conditions for Direct Computation of Aerodynamic Sound Generation

Tim Colonius,* Sanjiva K. Lele,† and Parviz Moin‡
Stanford University, Stanford, California 94305

Accurate computation of the far-field sound along with the near-field source terms associated with a free shear flow requires that the Navier-Stokes equations be solved using accurate numerical differentiation and time-marching schemes, with nonreflecting boundary conditions. Nonreflecting boundary conditions have been developed for two-dimensional linearized Euler equations by Giles. These conditions are modified for use with nonlinear Navier-Stokes computations of open flow problems. At an outflow, vortical structures are found to produce large reflections due to nonlinear effects; these reflection errors cannot be improved by increasing the accuracy of the linear boundary conditions. An exit zone just upstream of an outflow where disturbances are significantly attenuated through grid stretching and filtering is developed for use with the nonreflecting boundary conditions; reflections from vortical structures are decreased by 3 orders of magnitude. The accuracy and stability of the boundary conditions are investigated in several model flows that include sound radiation by an energy source in a uniformly sheared viscous flow, the propagation of vortices in a uniform flow, and the spatial evolution of a compressible mixing layer.

I. Introduction

COMPUTATION of both the far-field sound and near-field source terms associated with a turbulent free shear flow allows the sound generation process to be studied directly, that is, without modeling the source terms. The far-field sound may be measured experimentally, but the source terms for acoustic analogies, which are a function of an unsteady flowfield, are difficult to measure. In theoretical aeroacoustics, source terms are modeled and the far-field sound predicted. By solving the full unsteady Navier-Stokes equations, however, both the far-field sound and the near-field hydrodynamics are known, and such computations may then be used to validate theories and study the detailed physics of sound generation. Such knowledge will ultimately provide noise control strategies based on fundamental physics rather than empirical correlations.

Computations of free shear flows using the unsteady, compressible Navier-Stokes equations have been performed for some time. Typically, however, little effort is made to resolve the acoustic waves whose energy is many orders of magnitude smaller than the hydrodynamic field. In a recent review article, Crighton[1] cites three sources of difficulty in directly resolving the acoustic waves in Navier-Stokes computations: the large extent of the acoustic field compared with flowfield, the very small energy of the acoustic field compared with the flowfield, and the possibility that numerical discretization itself may act as a more significant source of sound than the continuous flowfield that is approximated. A fourth difficulty is the posing of the free space boundary conditions appropriate for the acoustic far field at an artificial computational boundary a finite distance away from the source region. These artificial boundaries not only must be appropriate for nonreflection of acoustic waves but also in certain regions must provide for inflow and outflow of the hydrodynamic field. We have considered a variety of model problems to directly address these issues. The present numerical method was used by the authors to study the scattering of sound waves by a compressible vortex.[2] In addition, the same method was used by Mitchell et al.[3] to compute the sound produced by a pair of corotating vortices, and a similar method was used by Lele and Ho[4] to compute the sound generated by a temporally evolving (periodic in the streamwise direction) compressible mixing layer. These previous computations gave good agreement with predictions based on acoustic analogies. The boundary conditions that were used, however, were accurate only for waves propagating in a single known direction at the computational boundary. In more general flows, such as free shear flows, such boundary conditions are not accurate. Since the directivity of the generated sound is not known in advance, boundary conditions accurate for incident waves over a range of angles are necessary. Inaccuracies also arise from the passage of large-scale vortical structures through the outflow. These difficulties can prevent the direct computation of sound generation by turbulent free shear flows by producing spurious acoustic waves of larger magnitude than the sound generated by the actual hydrodynamic sources. In this paper, we devote our attention to resolving these problems through the derivation of nonreflecting boundary conditions suitable for computations of spatially evolving free shear flows. We apply our techniques to several model problems: the sound radiated by an energy source in a uniformly sheared viscous flow, the propagation of vortices in a uniform flow, and the evolution of a two-dimensional spatially evolving mixing layer forced at its fundamental frequency.

II. Numerical Issues and Boundary Conditions

The fully compressible unsteady Navier-Stokes equations along with the equation of continuity and energy are to be solved numerically. For simplicity, the fluid is assumed to be a calorically perfect gas, with constant molecular properties. To accurately resolve the propagation of the acoustic waves, finite difference and time-marching schemes that have low numerical dissipation and accurately represent the dispersion relation for the inviscid equations are required. To this end, a sixth-order-accurate compact finite difference scheme[5] is chosen for evaluating spatial derivatives. This scheme has low dissipation and near spectral representation of the dispersion relationship. When spatial derivatives near the computational

*Research Assistant, Department of Mechanical Engineering. Student Member AIAA.

†Assistant Professor, Departments of Mechanical Engineering and Aeronautics and Astronautics.

‡Professor, Department of Mechanical Engineering; also Senior Staff Scientist, NASA Ames Research Center, Moffett Field, CA 94035. Associate Fellow AIAA.

boundaries are needed, a third-order-accurate compact scheme biased toward the interior nodes is used.[5] An explicit fourth-order Runge-Kutta time advancement is used to give low amplitude and phase errors of traveling wave solutions. The model flows considered have infinite extent in both spatial dimensions, and therefore finite artificial computational boundaries are introduced. The concept of nonreflecting boundary conditions proposed by Enquist and Majda[6,7] and subsequently modified by others[8-12] is used. Nonreflecting boundary conditions are typically derived for a linear system of hyperbolic equations, and hence boundary conditions for the linearized Euler equations such as those presented by Giles[12,13] need to be modified. In what follows, we restrict our attention to the case where the flow is everywhere subsonic. Consider the two-dimensional Navier-Stokes equations written in terms of the primitive variables, u, v, p, and ρ,

$$\frac{\partial u}{\partial t} + A\frac{\partial u}{\partial x} + B\frac{\partial u}{\partial y} = \mathbf{d} \tag{1}$$

where u and v are the velocities in the x and y directions relative to the speed of sound at some fixed reference location a_{ref}, ρ is the density relative to the density at the reference location ρ_{ref}, p is the pressure relative to $\rho_{\text{ref}}a_{\text{ref}}^2$, u is the solution vector $\{\rho\ u\ v\ p\}$, v is a vector containing the viscous terms (not written here for brevity), and

$$A = \begin{pmatrix} u & \rho & 0 & 0 \\ 0 & u & 0 & 1/\rho \\ 0 & 0 & u & 0 \\ 0 & \gamma p & 0 & u \end{pmatrix} \tag{2a}$$

$$B = \begin{pmatrix} v & 0 & \rho & 0 \\ 0 & v & 0 & 0 \\ 0 & 0 & v & 1/\rho \\ 0 & 0 & \gamma p & v \end{pmatrix} \tag{2b}$$

Now, assume that the flow is linearized about a time-invariant reference flow at the boundaries. The reference flow is not required to be an exact solution of the Navier-Stokes equations but is assumed to be "close" to a steady solution, such that the deviation between it and a steady laminar (or "mean") solution is small. Therefore, let

$$u = u_0(x,y) + u'(x, y, t) \tag{3}$$

which, upon substitution into Eq. (1) and neglecting terms of second order and higher in u' gives

$$\frac{\partial u'}{\partial t} + A_0\frac{\partial u'}{\partial x} + B_0\frac{\partial u'}{\partial y} + C_0 u' = v' + \mathcal{S}_0 \tag{4}$$

where $\mathcal{S}_0$ is a source term depending on the chosen reference flow,

$$\mathcal{S}_0 = \mathbf{d}_0 - A_0\frac{\partial u_0}{\partial x} - B_0\frac{\partial u_0}{\partial y} \tag{5}$$

and where

$$A_0 = \begin{pmatrix} u_0 & \rho_0 & 0 & 0 \\ 0 & u_0 & 0 & 1/\rho_0 \\ 0 & 0 & u_0 & 0 \\ 0 & \gamma p_0 & 0 & u_0 \end{pmatrix} \tag{6a}$$

$$B_0 = \begin{pmatrix} v_0 & 0 & \rho_0 & 0 \\ 0 & v_0 & 0 & 0 \\ 0 & 0 & v_0 & 1/\rho_0 \\ 0 & 0 & \gamma p_0 & v_0 \end{pmatrix} \tag{6b}$$

$$C_0 = \begin{pmatrix} \left(\frac{\partial u_0}{\partial x} + \frac{\partial v_0}{\partial y}\right) & \frac{\partial \rho_0}{\partial x} & \frac{\partial \rho_0}{\partial y} & 0 \\ \left(\frac{u_0}{\rho_0}\frac{\partial u_0}{\partial x} + \frac{v_0}{\rho_0}\frac{\partial u_0}{\partial y}\right) & \frac{\partial u_0}{\partial x} & \frac{\partial u_0}{\partial y} & 0 \\ \left(\frac{u_0}{\rho_0}\frac{\partial v_0}{\partial x} + \frac{v_0}{\rho_0}\frac{\partial v_0}{\partial y}\right) & \frac{\partial v_0}{\partial x} & \frac{\partial v_0}{\partial y} & 0 \\ 0 & \frac{\partial p_0}{\partial x} & \frac{\partial p_0}{\partial y} & \gamma\left(\frac{\partial u_0}{\partial x} + \frac{\partial v_0}{\partial y}\right) \end{pmatrix} \tag{6c}$$

If the reference flow is chosen to be uniform, then $C_0 = \mathcal{S}_0 = 0$ and in the absence of viscous effects, the system of Eq. (4) reduces to the linearized Euler equations considered in Refs. 6 and 12. In two dimensions, exactly nonreflecting boundary conditions may be derived in Fourier space by modifying the dispersion relation for the linear equations to prohibit wave propagation for waves with components of their group velocity directed into the computational domain. This modified dispersion relation is nonlinear, and thus the exactly nonreflecting physical space boundary conditions are necessarily nonlocal in both space and time (in one dimension, they are local). To produce local boundary conditions, the dispersion relation is expanded in a Taylor series (alternative expansions are also possible[6]) for small values of k_s/ω, where k_s is the spatial frequency in the direction parallel to the computational boundary, and ω is the temporal frequency. A resulting hierarchy of boundary conditions is reported by Giles.[12,13] The boundary conditions are written in terms of the one-dimensional characteristic variables, c, which are (for a boundary that is aligned with a line x = const)

$$c = \begin{pmatrix} c_1 \\ c_2 \\ c_3 \\ c_4 \end{pmatrix} = \begin{pmatrix} \dfrac{-\gamma p_0}{\rho_0} & 0 & 0 & 1 \\ 0 & 0 & \sqrt{\gamma\rho_0 p_0} & 0 \\ 0 & \sqrt{\gamma\rho_0 p_0} & 0 & 1 \\ 0 & -\sqrt{\gamma\rho_0 p_0} & 0 & 0 \end{pmatrix}\begin{pmatrix} \rho' \\ u' \\ v' \\ p' \end{pmatrix} \tag{7}$$

Physically, the four one-dimensional characteristic variables can be interpreted as the amplitude of entropy and vorticity waves (c_1 and c_2, respectively) that convect across the computational boundary with the component of the reference flow velocity normal to the boundary and acoustic waves that propagate downstream and upstream relative to the velocity normal to the boundary (c_3 and c_4, respectively).

For inflow the following boundary conditions are considered.

BCI1:

$$\begin{pmatrix} c_1 \\ c_2 \\ c_3 \end{pmatrix} = \begin{pmatrix} 0 \\ 0 \\ 0 \end{pmatrix} \tag{8}$$

BCI2:

$$\begin{pmatrix} c_1 \\ \dfrac{\partial c_2}{\partial t} \\ \dfrac{\partial c_2}{\partial t} \end{pmatrix} + \begin{pmatrix} 0 & 0 & 0 & 0 \\ 0 & v_0 & \dfrac{a_0 + u_0}{2} & \dfrac{a_0 - u_0}{2} \\ 0 & \dfrac{a_0 - u_0}{2} & v_0 & 0 \end{pmatrix}\frac{\partial}{\partial y}\begin{pmatrix} c_1 \\ c_2 \\ c_3 \\ c_4 \end{pmatrix} = \begin{pmatrix} 0 \\ 0 \\ 0 \end{pmatrix} \tag{9}$$

For outflow the following boundary conditions are considered.

BCO1:

$$c_4 = 0 \tag{10}$$

BCO2:

$$\frac{\partial c_4}{\partial t} + \left[0 \ (a_0 + u_0)/2 \ 0 \ v_0 \right] \frac{\partial}{\partial y} \begin{pmatrix} c_1 \\ c_2 \\ c_3 \\ c_4 \end{pmatrix} = 0 \qquad (11)$$

BCO3:

$$\frac{\partial c_4}{\partial t} + (0 \ u_0 \ 0 \ v_0) \frac{\partial}{\partial y} \begin{pmatrix} c_1 \\ c_2 \\ c_3 \\ c_4 \end{pmatrix} = 0 \qquad (12)$$

where $a_0 = \sqrt{\gamma p_0/\rho_0}$. We have actually changed the first equation of BCI2 from the specification of Giles[12]:

$$\frac{\partial c_1}{\partial t} + v_0 \frac{\partial c_1}{\partial y} = 0 \qquad (13)$$

Both equations give the same accuracy in terms of reflection coefficients.

Numerically, the outgoing characteristic variables (i.e., c_4 at an inflow and c_1, c_2, and c_3 at an outflow) must also be computed. Typically this is accomplished by extrapolating their value from the interior node points or by computation via the full equations using one-sided finite differences to approximate the spatial derivatives. We choose the latter approach in the problems considered here. To do this, the transformation given by Eq. (7) is applied to the linearized equations (4). The equations are advanced in time with a fourth-order Runge-Kutta scheme as in the interior of the domain, whereas the spatial derivatives use a third-order Padé scheme biased toward the interior nodes given by Lele.[5]

The aforementioned boundary conditions of Eqs. (8–13) are written for a plane boundary aligned with a coordinate axis. The derivirtives transverse to the boundary that appear in the boundary conditions are finite differenced in the same manner as described earlier, that is, with a sixth-order Padé scheme in the interior of the boundary and the third-order biased scheme at the corners. A significant practical problem that we do not consider in detail is the posing of the boundary conditions at corner points in computational domains. In what follows, we have chosen to apply the preceding boundary conditions at an angle that bisects the two coordinate directions at the corner, as is suggested by Enquist and Majda.[6]

One way to measure accuracy of the preceding boundary conditions is with reflection coefficients, which are defined as the ratio of a particular incoming (reflected) wave to a particular outgoing wave. At an inflow, for example, there are three reflection coefficients: acoustic to entropy, acoustic to vorticity, and acoustic to acoustic. At an outflow, there are also three reflection coefficients: entropy to acoustic, vorticity to acoustic, and acoustic to acoustic. For the boundary conditions BCI1 and BCO1, all of the reflection coefficients except those involving entropy are proportional to $\Theta(k_s/\omega)$ (they are therefore known as first-order boundary conditions or, alternatively, zeroth-order conditions since the dispersion relation for this case is truncated to zeroth order). The reflection coefficient involving entropy is 0 for BCI1 and BCO1. The acoustic-acoustic reflections generated when BCI2 or BCO2 is used are zero to $\Theta(k_s/\omega)$ (Ref. 4), whereas they are zero to $\Theta(k_s/\omega)^2$ for BCO3. The vorticity-acoustic reflection for BCO2 is proportional to (k_s/ω), whereas it is 0 for BCO3. The previous statements are only correct to the extent that the disturbances u' are indeed small such that the linearization in Eqs. (4) is accurate.

In applying the boundary conditions of Eqs. (8–12) to flows where the reference flow is not uniform, we use the local value of the reference flow u_0, and it is therefore assumed that the perturbation field varies on a length scale much shorter than the reference field. This assumption can be violated in a variety of situations, and therefore we have devoted a significant amount of attention to establishing the accuracy of the boundary conditions empirically. Additionally, we note that using boundary conditions BCI1 and BCI2 for the inflow boundary in Navier-Stokes solutions represents a significant departure from commonly used methods where, typically, the full instantaneous velocities and, say, temperature are fixed for all time. In the current formulation, the inflow conditions are set only approximately by the reference flow and are allowed to fluctuate to allow upstream propagating acoustic waves to leave the computational domain. If the overall system is stable, then the reference inflow conditions u_0 are modified only to the extent that the mean of the upstream propagating disturbances is nonzero; this should typically be quite small.

III.   Stability and Accuracy of Boundary Conditions

The analysis performed by Giles[12,13] shows that the boundary conditions BCI1, BCI2, BCO1, BCO2, and BCO3 are well posed for the continuous Euler equations linearized about a uniform mean flow, $u_0 = \text{const}$, for a single computational boundary. Similar boundary conditions were also studied by Gustaffson,[11] who claims that they are at least weakly ill posed in the sense of Kreiss.[14] Even if they are well posed, well-posedness for the more general nonlinear problem with multiple boundaries is not guaranteed.[15] Even if the problem is well posed, instabilities may arise when the continuous system is discretized.

Numerical experiments of random perturbations added to a uniform mean flow show that the perturbations are damped over time and that the solution relaxes to the uniform mean flow to round-off accuracy as long as the Courant-Friedricks-Levy (CFL) number is suitably small. (In fact, the stability limit CFL < 1.4 predicted by a stability analysis of the current scheme for a one-dimensional periodic advection equation given in Ref. 5 was reasonably well obeyed.) However, perturbations in sheared flow (which will be described shortly) with boundary conditions BCI2 and BCO2 or BCO3 are not damped, and the L_2 norm of the solution eventually grows exponentially in time. Since this instability is apparently due to the shear, the usual analytical stability analyses that depend on constant coefficient equations are not particularly useful.

For guidance in stabilizing the numerical scheme for flows with mean shear, a full matrix linear stability analysis is performed. By full matrix analysis we mean the computation of the eigenstructure of the matrix M that results when the entire numerical scheme for two-dimensional problems (including boundary conditions) is written in the form

$$\hat{u}^{n+1} = M\hat{u}^n \qquad (14)$$

where $\hat{u}^n$ is a vector of the spatially discretized values of primitive variables u' at time level n. The matrix M is a square $N \times N$ matrix, where $N = N_x \times N_y \times 4$, and therefore determining its eigensystem is only possible for small numbers of grid points. Also, M is a function of the reference flow u_0, the choice of spatial-differencing and time-marching schemes, the boundary conditions, and the particular grid resolution and time step used. The observed instability indicates that M will have at least one eigenvalue with magnitude greater than one.

The uniformly sheared viscous reference flow is given by

$$u_0 = \begin{pmatrix} \rho_0 \\ u_0 \\ v_0 \\ p_0 \end{pmatrix} = \left\{ \begin{matrix} [1 - (\gamma - 1)PrS^2y^2/2]^{-1} \\ M + Sy \\ 0 \\ 1/\gamma \end{matrix} \right\} \qquad (15)$$

where S is the shear rate, and M is the Mach number at $y = 0$. The computational domain for Eq. (15) is rectangular, extending from 0 to $x_{\max}$ in x and from $-y_{\max}$ to $+y_{\max}$ in y. Note

that Eq. (15) is an exact solution of the compressible Navier-Stokes equations, but to avoid nonphysical negative temperatures, $S < 2.582/y_{max}$ (for $\gamma = 1.4$ and $Pr = 1.0$).

The eigenvalues of M were found using a double precision eigenvalue routine with iterative refinement on the CRAY Y-MP computer. The accuracy of the eigenvalues was checked in two ways. The computed eigenvectors and eigenvalues were used to recompute the matrix, which was compared with the original matrix M, and the numerical solutions for unstable cases were compared with the predicted most unstable eigenvector. We believe the eigenvalues quoted next are accurate to (at least) the precision reported.

When $S = 0$, Eq. (15) is a uniform flow, and the eigenvalues of M are found to have magnitude less than 1 for any of the boundary conditions of Eqs. (8–12), as long as the CFL restriction is obeyed. When $S \neq 0$, using BCI1 and BCO1 also gives eigenvalue magnitudes less than 1. However, when BCI2 and BCO2 or BCO3 are used, eigenvalues with magnitude greater than 1 are obtained. Figure 1 shows a typical plot of the eigenvalue magnitudes in the complex plane for the case $N_x = N_y = 17$, $y_{max} = 1$, $x_{max} = 2$, $Pr = 1.0$, $S = 0.125$, $M = 0.375$, and $\Delta t = 0.004$, with BCI2 and BCO2. The maximum eigenvalue magnitude for this case is 1.000020.

To stabilize the shear flow computations, damping terms are added to the left-hand side of boundary conditions BCI2 and BCO2 or BCO3. For the inflow, the damping term is of the form

$$\begin{bmatrix} 0 & 0 & 0 & 0 \\ 0 & 0 & 0 & 0 \\ 0 & 0 & \epsilon/2 & -\epsilon/2 \end{bmatrix} \begin{bmatrix} c_1 \\ c_2 \\ c_3 \\ c_4 \end{bmatrix} \quad (16)$$

whereas for the outflow it is of the form

$$(0 \ \ 0 \ \ \epsilon/2 \ \ \epsilon/2) \begin{bmatrix} c_1 \\ c_2 \\ c_3 \\ c_4 \end{bmatrix} \quad (17)$$

The form of these terms is chosen so that they drive the flow toward $c = 0$ or equivalently toward the reference flow u_0. For small ϵ, the additional term causes the magnitude of the reflection coefficients discussed earlier to be changed only for the reflected acoustic wave at the inflow and outflow; the order of vortical and entropic reflections at the outflow remains the same. The additional reflected acoustic wave is proportional to ϵ. Ideally, the value of ϵ should be small with respect to the reflection errors that arise from the truncation of the modified dispersion relation, so that the nonreflecting properties of the boundary conditions are not significantly degraded.

Damping terms similar to the ones proposed earlier were included in the boundary condition treatments of Poinsot and Lele[16] and Rudy and Strikwerda,[17] who discuss a physical interpretation and the parametric dependence of the constant ϵ and show that the value of the constant scales with the inverse of length of the computational domain in the direction normal to the boundary; i.e., larger domains require smaller amounts of damping.

When Eqs. (16) and (17) are added to BCI2 and BCO2, the resulting maximum eigenvalue magnitude of M is less than 1 for a suitably large value of ϵ. Figure 2 shows that maximum eigenvalue magnitude as a function of ϵ for the same case as Fig. 1. The threshold value of ϵ above which stable numerical schemes are obtained is about 0.001 for this case. Numerical experiments on the shear flow with $\epsilon > 0.001$ indicate that the CFL limit predicted by the simple periodic one-dimensional advection equation analysis is once again roughly obeyed.

We note that the preceding matrix stability analysis was performed to demonstrate that the proposed damping is a viable way to remove the observed instability in the computations. It should not be interpreted as a general stability analysis of the current scheme and is not particularly useful for predicting CFL restrictions due to its large computational expense. Similarly, the value of ϵ quoted earlier is valid only for the particular parameters used. We do not recommend this particular value of ϵ for other problems, since the dependence of ϵ on the relevant physical and numerical parameters was not thoroughly investigated. In the remainder of the test cases considered, we have used a larger amount of damping, $\epsilon = 0.05$, which we find to be a fairly robust value in that stability is achieved for all of the problems we have considered.

To investigate the accuracy of the higher order boundary conditions discussed earlier, both with and without the damping, the generation of acoustic waves by a source in the uniformly sheared viscous flow is computed. Acoustic waves are generated by placing a quadrupole time harmonic energy source in the center of the computational domain. A schematic diagram of the flow and computational domains used is shown in Fig. 3. In both the x and y directions, grid points were used, which gives approximately 40 grid points per acoustic wavelength, which is sufficient resolution to keep the discretization errors much smaller than the errors due to the approximations in the boundary conditions. The CFL number for the computation was 0.7. For several different boundary conditions Fig. 4 shows a comparison of pressure fluctuations produced by the source after several wavelengths of the generated sound have crossed the computational boundary: 1) higher order inflow and outflow (BCI2 and BCO2) with $\epsilon = 0$,
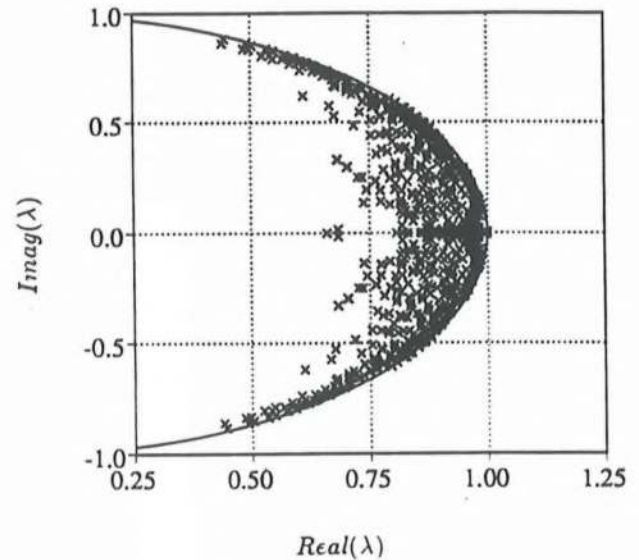

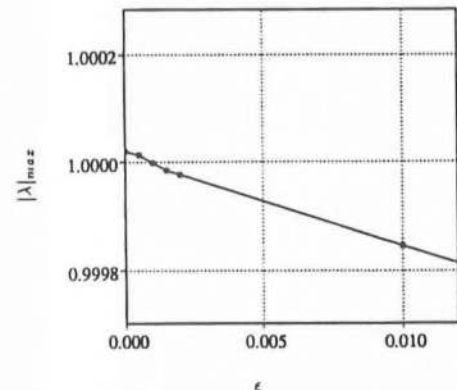Fig. 1   Location of the eigenvalues of M in the complex plane; the solid line is the unit circle.

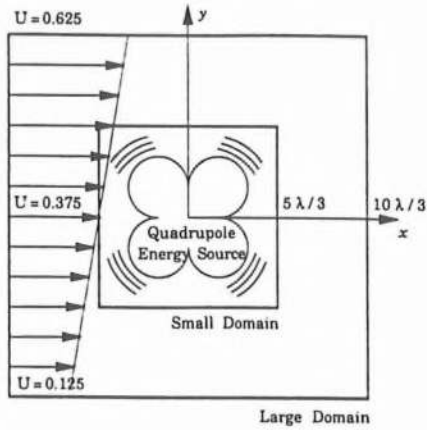Fig. 2   Maximum eigenvalue magnitude as a function of the damping parameter ϵ.

Fig. 3 Schematic diagram of quadrupole sound generation in uniformly sheared flow.
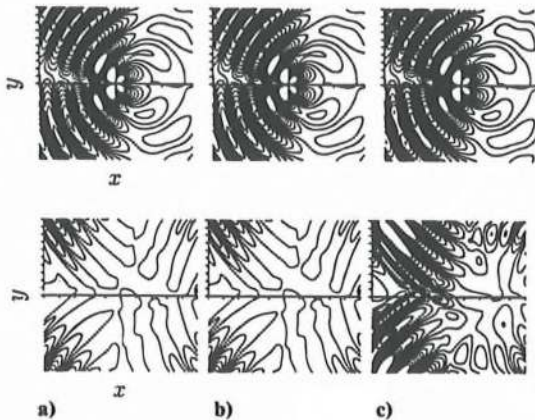

Fig. 4 Comparison of boundary conditions; the top row shows isocontours of pressure fluctuations, and the bottom row shows isocontours of the error in pressure fluctuations: a) BCI2, BCO2, $\epsilon = 0$; b) BCI2, BCO2, $\epsilon = 0.05$; and c) BCI1 and BCO1. Contour levels in the top row are min = -5×10^{-5}, max = 5×10^{-5}, and increment = 5×10^{-6}, and in the bottom row they are min = -5×10^{-6}, max = 5×10^{-6}, and increment = 5×10^{-7}.

2) BCI2 and BCO2 with $\epsilon = 0.05$, and 3) first-order inflow and outflow (BCI1 and BCO1). The instantaneous pressure fields are plotted in the top row of the figure, and the difference between the top row and the "exact solution" is plotted in the bottom row. The exact solution is obtained from a computation performed on the larger computational domain, where reflection errors from the boundaries have not had sufficient time to contaminate the solution inside the smaller box size. The reflection errors for BCI2 and BCO2 are an order of magnitude smaller than the reflection errors from BCI1 and BCO1. The effect of the additional damping terms on the waves is apparently very small.

After some time, the energy source is turned off to determine the boundary conditions' ability to allow the flow to return to the steady reference flow. Figure 5 shows the root mean square streamwise velocity fluctuation (averaged over the computational domain) as a function of time (note the log scale in the figure) after the source has been turned off. An exponential type of instability is evident for BCI2 and BCO2 with $\epsilon = 0$, whereas the fluctuations die off to machine zero when the damping is used. It is interesting to note that the rate of the exponential growth of the unstable scheme is nearly 1 when time is normalized with the time it takes a particle to traverse the computational domain. This suggests a feedback resonance between the inflow and outflow boundaries as the mechanism for the instability. We will have more to say about this feedback in connection with the spatially evolving mixing layer considered in Sec. V.

IV. Propagation of Vortices in Uniform Flow

We next consider the propagation of a vortex in a uniform flow, as it travels through the computational outflow boundary. This problem is chosen to test how the boundary conditions discussed earlier handle a large convecting disturbance that violates the linearity assumed in the boundary condition derivation. The computations are initialized with a compact, zero circulation vortex[18] in the center of the computational domain. The vortex then convects with the uniform flow and eventually travels through the outflow boundary, generating a reflected acoustic wave. In both the x and y directions, 200 grid points were used for this computation, and the CFL number was 0.7. Figure 6 shows this process for a computation where the outflow conditions BCO3 were used. It is clear that the outflow boundary condition is satisfactory for the vorticity (hydrodynamic) field, but it is inadequate for the acoustic field.

We have run this test for both boundary conditions BCO2 and BCO3, varying the amplitude of the vortex relative to the uniform flow. The results are shown in Fig. 7, where the maximum amplitude of the dilatation in the reflected acoustic wave is plotted against the amplitude of the incident vortex (defined as the maximum vorticity in the vortex). According to the previous discussion of reflection coefficients, BCO2 should produce a reflection that is proportional to (k_s/ω) times the incident vortex. Since (k_s/ω) is held fixed as the amplitude varies, Fig. 7 gives a linear variation of the reflected acoustic wave amplitude with the incident vortex amplitude for BCO2. According to the analysis, BCO3 should produce no vortex-acoustic reflection, but Fig. 7 shows a reflected acoustic wave that is proportional to the square of the ampli-
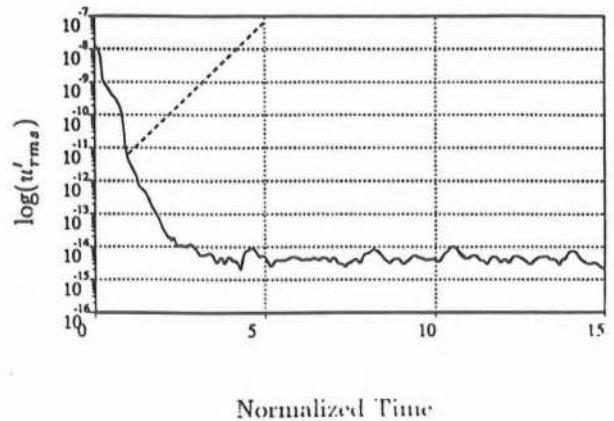

Normalized Time

Fig. 5 Comparison of boundary conditions, decay of streamwise velocity fluctuations in uniformly sheared flow after acoustic source is turned off. Time is normalized by the average time for a particle to traverse the computational domain: ——, BCI2, BCO2, and $\epsilon = 0.05$; $----$, BCI2, BCO2, and $\epsilon = 0$.

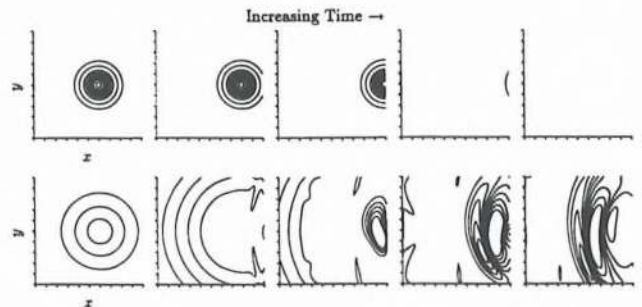**Fig. 6 Acoustic wave reflection by vortex propagating through outflow boundary. In the top row, the isocontours of vorticity are min = -0.1, max = 0.8, and increment = 0.05. In the bottom row, the isocontours of the dilatation are min = -0.01, max = 0.01, and increment = 0.001.**

tude of the incident vortex. This is due to nonlinear effects that are neglected in the boundary condition treatment. Since the two curves for BCO2 and BCO3 approach each other for large vortex amplitudes, there is no advantage to the more accurate boundary condition when the outflowing disturbances are not small compared with the reference flow. Typically the sound radiated by flow structures is many orders of magnitude smaller than the hydrodynamic fluctuations, and a reflection of the magnitude given by Fig. 7 would completely obscure the sound generation process.

We now proceed to modify the outflow boundary conditions to reduce the magnitude of the acoustic reflection due to the passage of large vortical disturbances. One approach that has been successful in direct numerical simulations of hydrodynamic fields (see, for example, Rai and Moin[19]) is the use of an exit zone, where the grid becomes coarse in the downstream direction, and filtering and/or artificial viscosity are used to damp disturbances as they propagate through the coarse mesh. Typically this approach is coupled with a crude boundary condition at the downstream boundary of the exit zone, such as the specification of the pressure, and extrapolation of the other flow variables. The exit zone works as follows: disturbances that are propagating downstream into the region of grid stretching become less well resolved. Upwind/downwind biased differentiation schemes have the property of significantly attenuating disturbances that are poorly resolved on the computational mesh, and so the disturbances are significantly damped before they interact with the downstream computational boundary. Similarly, a nonbiased differentiation scheme can be used if the field is low pass filtered in the region of the grid stretching, such that unresolved disturbances are attenuated.

There are two potential problems with such an approach. First, the least resolved disturbances can propagate upstream; it is thus possible that the solution upstream will become contaminated with small wavelength disturbances. Second, grid stretching produces acoustic waves that propagate both upstream and downstream.

Consider, for example, the following grid-stretching scheme. Let the variable s represent a uniform grid that extends from 0 to s_{max}, with N grid points (including the endpoints). Let Δs be grid spacing in s [such that $s_{max} = (N-1)\Delta s$] and let the initial physical domain grid spacing also be also equal to Δs. Let x_p and x_{max} be the desired coordinates of the end of the physical domain and the complete length of the computational domain, respectively. Finally, let Δx_p and Δx_{max} be the (stretched) grid spacing at x_p and x_{max}, respectively. The physical coordinate x is given by

$$x = s + \frac{\Delta x_{max}}{\sigma \Delta s} \ell n[e^{\sigma(s-s_t)} + 1] \qquad (18)$$
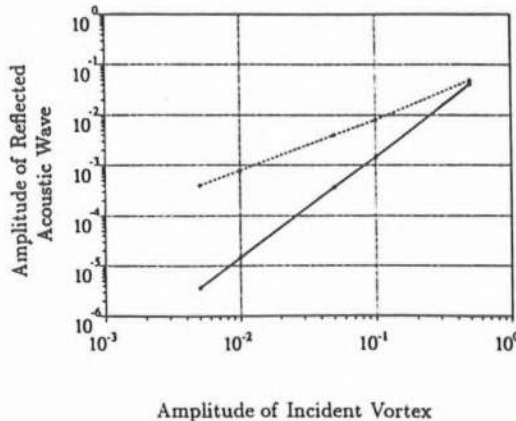

Fig. 7 Reflected acoustic wave as a function of the amplitude of the incident vortex: —— , BCO3; - - - - , BCO2.
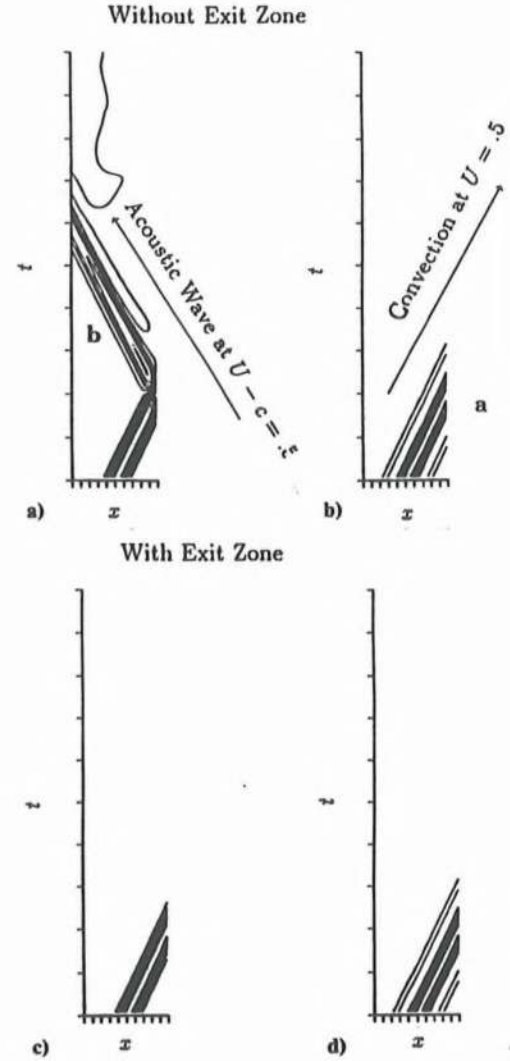

Fig. 8 Propagation of a vortex in uniform flow, $M = 0.5$; comparison of computations with and without exit zones on x-t diagrams. Shown are contours of a) pressure without exit zone, b) vorticity without exit zone, c) pressure with exit zone, and d) vorticity with exit zone. Boldface letters refer to specific events mentioned in the text. All computations with BCI2 and BCO3. Contours: pressure— min = 71.368, max = 71.459, increment = 0.007; vorticity—min = −2.0, max = 0.8, increment = 0.4.

where

$$s_t = \frac{s_{max}[1 + (\Delta x_{max}/\Delta_s)] - x_{max}}{(\Delta x_{max}/\Delta_s)} \qquad (19)$$

$$\sigma = \frac{\ell n(\Delta x_{max}/\delta \Delta_s)}{s_t - x_p} \qquad (20)$$

$$\delta = \frac{\Delta x_p}{\Delta_s} - 1 \qquad (21)$$

The parameter δ controls how much the grid has been stretched by x_p, the end of the physical domain. The closer δ is to 0, the more uniform the mesh is in the physical region. We have used $\delta = 0.00001$, which gives a very smooth transition to the coarser mesh in the region near $x = x_{max}$.

We chose to filter the solution in the exit zone. An explicit filter of the form

$$\hat{f}_i = a(x)f_i + b(x)(f_{i+1} + f_{i-1}) + c(x)(f_{i+2} + f_{i-2}) \qquad (22)$$

where $\hat{f}_j$ is the filtered field at point s_j; and the coefficients a, b, and c vary smoothly (with the ratio of the local grid spacing
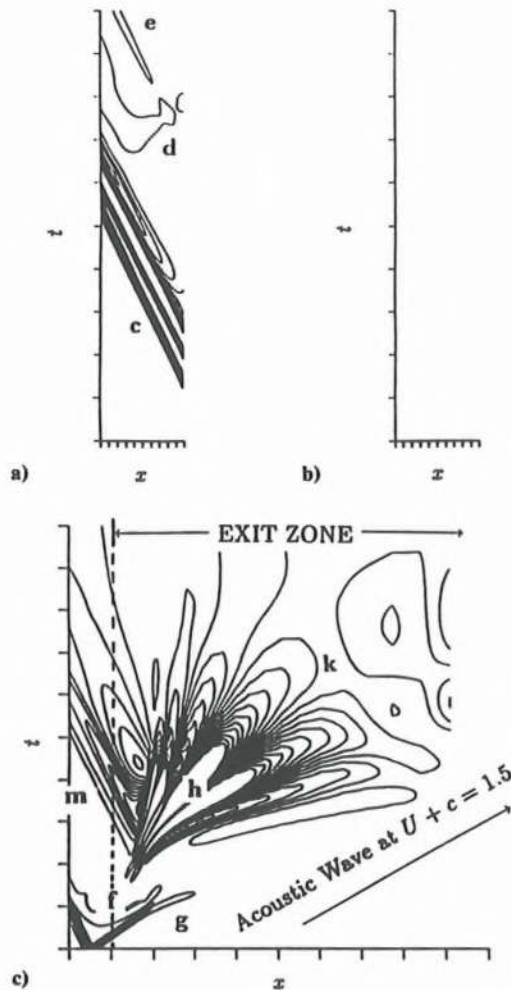
Fig. 9 Propagation of a vortex in uniform flow, $M = 0.5$; comparison of computations with and without exit zones on x-t diagrams. Shown are contours of a) dilatation without exit zone, b) dilatation with exit zone (levels: min $= -0.02$, max $= 0.02$, increment $= 0.002$), and c) contours of dilatation including exit zone (levels: min $= -0.0002$, max $= 0.0002$, increment $= 0.00002$). Boldface letters refer to specific events mentioned in the text.

to the initial grid spacing) from their values of 1, 0, and 0, respectively, in the physical region to 5/8, 1/4, and $-1/12$ at the end of the exit zone. This filter preserves at least second-order accuracy at all points in the exit zone but significantly attenuates poorly resolved disturbances throughout only the exit zone. We have used the following functions for the coefficients:

$$a(x) = \frac{5}{8} + \frac{3}{8}\left\{\exp\left[1 + \frac{\ell_n(\delta)(x - x_t)}{x_p - x_t}\right]\right\}^{-1} \tag{23a}$$

$$b(x) = \frac{2}{3}[1 - a(x)] \tag{23b}$$

$$c(x) = \frac{1}{6}[a(x) - 1] \tag{23c}$$

where x_t is the value of x where the ratio of the local grid spacing to the initial grid spacing is 1.25. These particular coefficients provide filtering throughout the exit zone only.

Any of the boundary conditions BCO1, BCO2, or BCO3 can be used at the end of the exit zone without modification.

To test the exit zone method, computations of vortex propagation in uniform flow were made on a domain with exit zone and compared with the computations discussed in the previous

section. The results are presented in Figs. 8 and 9, in the form of x-t diagrams that allow the reflection process to be seen clearly. The quantities shown in the figures are first integrated in the direction normal to the vortex propagation, and then isocontours are plotted in the x-t plane. Note that the integration in the normal direction produces no overall cancellation of waves, since the waves (as well as the vortex) are symmetric about the line $x = 0$. Sample characteristic path lines for both convective and propagating acoustic disturbances are shown in Fig. 8. Figure 8 shows the same pressure and vorticity contours for computations both with and without the exit zone. The convection of the vortex with the uniform flow is clearly seen in both the vorticity and pressure contours (the pressure is lower than ambient in the core of the vortex). This event is labeled as **a** in the figure. As the vortex reaches the end of the domain for the case without the exit zone, a large acoustic reflection is generated, which can be seen in the pressure contours (event **b**). At the contour levels shown in the figure, no reflection is evident for the computation with the exit zone.

The dilatation field is shown in Fig. 9 for both computations. The acoustic reflection from the vortex is evident for the case without the exit zone (event **c**). Multiple reflections continue as the time increases (events **d** and **e**). Shown in Fig. 9c is the dilatation field for the exit zone computation, but with contour levels 100 times smaller than in Fig. 9b. In Fig. 9c, the contours are also drawn in the exit zone, and the time scale has been expanded. At the smaller contour levels, an initial acoustic transient that propagates out from the initial vortex location (event **f**) is evident. This initial acoustic transient dies off sharply as it reaches the region of grid stretching and filtering (event **g**), without generating any appreciable propagating disturbance. As the vortex convects into the region of grid stretching and filtering, large dilatational disturbances are created (event **h**), and they are attenuated as they propagate further toward the end of the exit zone (event **k**). An upstream propagating acoustic wave is also created that travels into the physical domain (event **m**). The magnitude of this disturbance is quite small, about 3 orders of magnitude smaller than the reflected acoustic wave (event **c**) for the case without the exit zone. It is clear that the exit zone feature should be used when disturbances whose amplitude is not small compared with the reference flow are present.

We note that the additional cost for the exit zone for the proceeding problem is high, requiring roughly as many grid points in the exit zone as in the physical region. In general, however, the region need only be slightly larger than the largest flow structures which convect into it. Therefore, for spatially evolving shear flow computations, where the physical domain is generally much longer than the flow structures, the relative cost of the exit zone is small.

V. Two-Dimensional Mixing Layer

We now proceed to apply the methods developed in the previous sections to computations of a planar spatially evolving compressible mixing layer. We start our computation with a reference flow u_0, which is a solution to the laminar boundary-layer equations. This solution is determined by solving the Blasius equation with a shooting scheme described by Sandham and Reynolds.[20] For some of the computations, the solution is forced at the inlet by eigenfunctions determined by linear stability analysis of the laminar flow.[20] The reference flow pressure is uniform, and the temperature ratio across the layer is taken to be 1. In what follows, lengths are normalized by the initial vorticity thickness of the layer δ_ω (normalized to 1 in the computations). The velocities and density are normalized by the value of the streamwise velocity U_1 and density ρ_1 on the high-speed side of the layer, respectively.

At the computational boundaries in the normal (y) direction, there is inflow due to entrainment by the layer. The deviations from the reference flow are likely to be small at the inflow boundaries (both at the streamwise inflow boundary
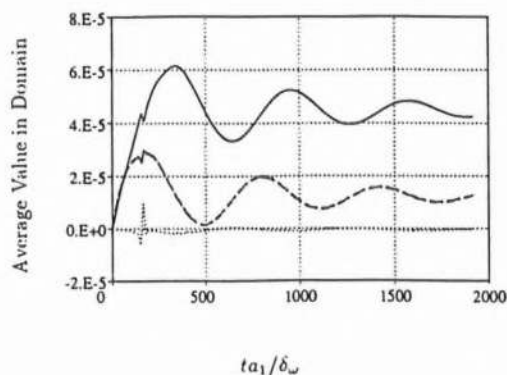
Fig. 10   Change in average u, v, ρ, and p in computational domain as a function of time: ——, u; ...., v; - - - -, ρ; —·—,p (lines for ρ and p fall directly on top of one another). Mixing layer with streamwise length of $x = 60\delta_\omega$. The small bump in the curves near $ta_1/\delta_\omega = 160$ is due to the passage of the startup vortex through the outflow boundary.
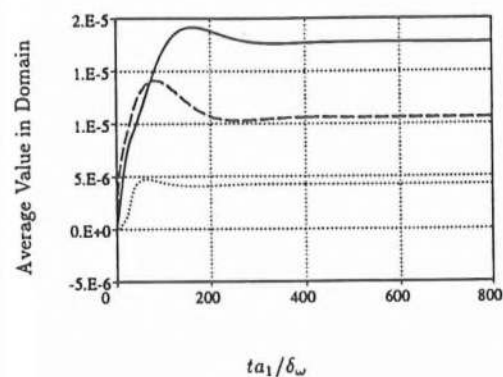
Fig. 11   Change in average u, v, ρ, and p in computational domain as a function of time: ——, u; ...., v; - - - -, ρ; —·—,p (lines for ρ and p fall directly on top of one another). Mixing layer with streamwise length of $x = 10\delta_\omega$.
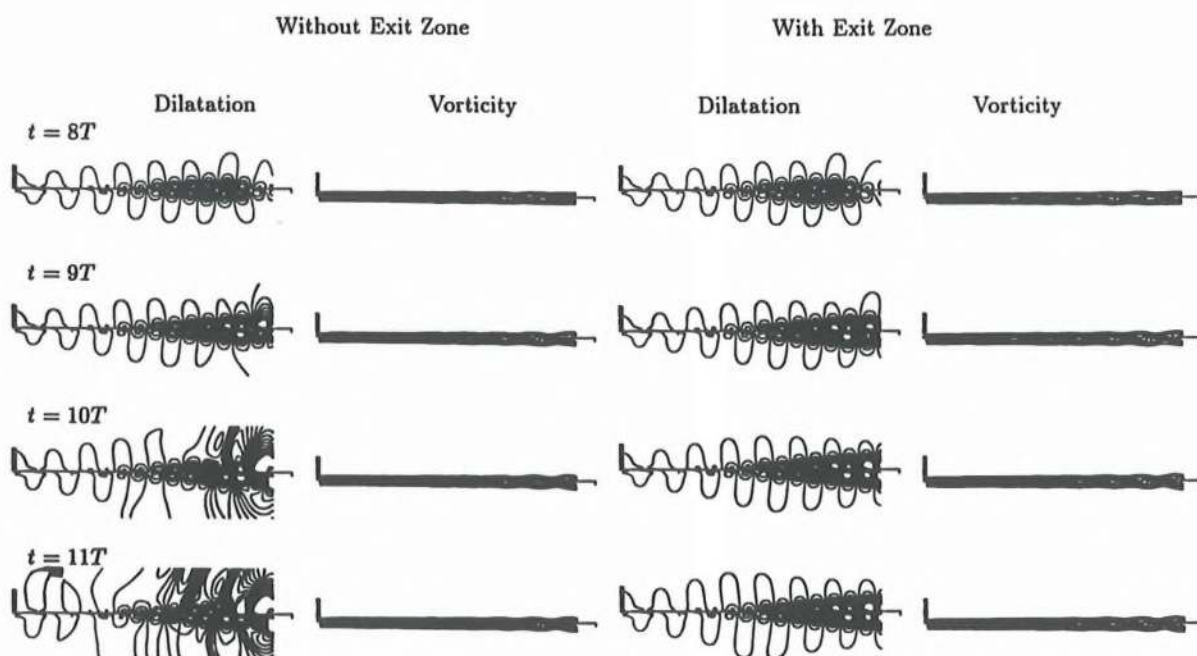

Fig. 12   Comparison of boundary conditions, mixing layer. Same parameters as before, except $x_p = 55\delta_\omega$. Contour levels: dilatation—min $= -3 \times 10^{-4}$, max $= 3 \times 10^{-4}$, and increment $= 3 \times 10^{-5}$; vorticity—min $= -0.25$, max $= -0.01$, and increment $= 0.03$. The T is one period of the fundamental frequency.

and the normal boundaries), owing solely to acoustic fluctuations, and therefore BCI2 is applied at these boundaries. At the outflow boundary, large flow structures must pass through the computational boundary, and therefore BCO3 is used in combination with the exit zone discussed in the previous section.

One problem that has been noted[21] in computing spatially evolving mixing layers (or indeed any convectively unstable flow) is self-forcing due to the coupling between the instabilities of the flow and the reflection process at the inflow/outflow boundaries. In addition to "physical" reflections that occur at artificial computational boundaries, artificial computational boundaries also produce short wavelength "sawtooth" reflections due to modifications in finite difference schemes necessary near and at the boundary. These reflections have been studied in detail by Vichnevetsky and Pariser[22] and Vichnevetsky.[23] By physical reflections, we mean smooth reflections produced by the inexactness of the nonreflecting boundary conditions. The sawtooth waves produced at the boundaries propagate upstream at speeds that can be greater than the sonic velocity and interact with the upstream

boundary, which reflects them as smooth, physical waves.[15]

For flows that do not amplify or damp physical disturbances as they propagate downstream, a numerical scheme can only be stable if the physical wave produced by the interaction of the sawtooth wave at the inflow has a smaller amplitude than the wave that originally produced the sawtooth wave at the outflow. In other words, the overall "reflection coefficient" must be less than 1. For convectively unstable flows, however, the smooth wave produced at the inflow may grow substantially, depending on its wavelength. Thus the product of the reflection coefficient and the total amplification of the disturbance as it convects through the computational domain must be less than 1. If this condition is not met, the mixing layer becomes self-forced, and the convective instability of the flow is turned into a global instability of the numerical method that has the appearance of a physically plausible solution.

The presence of such an instability may be tested by determining whether a computation fails to relax to steady state in the absence of continuous forcing. The initial conditions are not an exact solution to the Navier-Stokes equations and thus provide the initial disturbance for the instability. Figure 10

shows the change in the average values of u, v, ρ, and p in the computational domain as a function of time for one such computation. The Mach number of the high-speed stream is 0.5, the velocity ratio across the layer is 0.5, and the Reynolds number, $Re = (U_1 - U_2)\delta_\omega/d_1$, is 5×10^2. The domain extends to $60\delta_\omega$ in the streamwise direction, which is long enough for a 0.1% disturbance (relative to the reference velocity U_1) at the most unstable frequency to saturate before convecting out of the domain. The domain extends to $\pm 5\delta_\omega$ in the normal direction, and 601×101 grid points are used. The CFL number was, again, 0.7 (a similar computation with less resolution, 401×75 grid points, gave nearly identical results). The solution is apparently relaxing to steady state since the oscillations are damping over time. Figure 11 shows a computation on a shorter domain, extending to $10\delta_\omega$ (with 101×101 grid points), which relaxes to steady state much more rapidly. The damping parameter ϵ was 0.05 for both cases.

The necessity of the exit zone is also demonstrated by the mixing-layer computations. The parameters of the runs are the same as before, except that the physical domain extends to $55\delta_\omega$ for both cases. The computations are forced by the linear eigenfunctions corresponding to the most unstable frequency, at an amplitude of 0.1% at the inflow. Figure 12 shows a time series of plots of both the vorticity and dilatation for two runs, with and without exit zones. The time series shown corresponds to the time when the first vortex created by the eigenfunction forcing reaches the outflow boundary for the case without the exit zone. The time increment between each successive frame in Fig. 12 is one period of the most unstable frequency. Although the vorticity for the two runs appears to be identical, a large reflection is clearly evident in the contours of dilatation for the computation without the exit zone. The amplitude of the reflection is of the same order of magnitude as the maximum dilatation of the structures. It is obvious that such a strong acoustic reflection would obliterate any sound waves that the structures might produce. On the other hand, the reflection is not seen for the computation with the exit zone (and does not appear at later times that are not shown in the figure).

VI. Summary

In previous studies by Colonius et al.,[2] Mitchell et al.,[3] and Lele and Ho,[4] accurate computations of aerodynamic sound generation and the scattering of sound were performed for some model aeroacoustic problems. The results showed good agreement with both aeroacoustic theory and experimental evidence. In this paper we have described modifications to our numerical scheme and to the nonreflecting boundary conditions derived by Giles[12,13] to extend the method to allow accurate computations of free shear flows with inflow/outflow type boundaries.

To produce stable numerical schemes in the presence of shear, damping terms must be added to the boundary conditions. The amount of damping necessary to stabilize the system was found to be small and does not significantly alter the nonreflecting properties of the boundary conditions.

The accuracy of the outflow boundary condition, in terms of acoustic reflections from vortical disturbances, is controlled by nonlinear effects rather than the accuracy of the linear nonreflecting boundary condition for disturbance amplitudes expected in typical shear flow computations. An exit zone region where disturbances are significantly attenuated through grid stretching and filtering is developed. The use of such an exit zone is found to reduce the magnitude of acoustic reflections by 3 orders of magnitude for the flows studied. Computations of spatially evolving mixing layers without such an exit zone are shown to have acoustic reflections that completely obscure any other sound that may be produced by the flow. The current numerical method and boundary conditions were found to give stable results for computations of spatially evolving mixing layers; numerical self-excitation of the layer did not occur.

References

[1]Crighton, D. G., "Goals for Computational Aeroacoustics," *Computational Acoustics: Algorithms and Applications, Proceedings of the 1st IMACS Symposium on Computational Acoustics*, Elsevier Science Publishers, Amsterdam, 1986.

[2]Colonius, T., Lele, S. K., and Moin, P., "Scattering of Sound Waves by a Compressible Vortex," AIAA Paper 91-0494, Jan. 1991.

[3]Mitchell, B. E., Lele, S. K., and Moin, P., "Direct Computation of the Sound from a Compressible Co-Rotating Vortex Pair," AIAA Paper 92-0374, Jan. 1992.

[4]Lele, S. K., and Ho, C. M., "Acoustic Radiation from Temporally Evolving Free Shear Layers," Stanford Univ., Dept. of Aeronautics and Astronautics, Stanford, CA, 1991; also *Journal of Fluid Mechanics* (submitted for publication).

[5]Lele, S. K., "Compact Finite Difference Schemes with Spectral-Like Resolution," Center for Turbulence Research, Stanford Univ., CTR Manuscript 107, Stanford, CA, 1991; also *Journal of Computational Physics* (to be published).

[6]Enquist, B., and Majda, A., "Absorbing Boundary Conditions for the Numerical Simulation of Waves," *Mathematics of Computation*, Vol. 31, No. 139, 1977, pp. 629–651.

[7]Enquist, B., and Majda, A., "Radiation Boundary Conditions for Acoustic and Elastic Wave Calculations," *Communications on Pure and Applied Mathematics*, Vol. 32, No. 3, 1979, pp. 313–357.

[8]Higdon, R. L., "Absorbing Boundary Conditions for Difference Approximations to the Multi-Dimensional Wave Equation," *Mathematics of Computation*, Vol. 47, No. 176, 1986, pp. 437–459.

[9]Higdon, R. L., "Numerical Absorbing Boundary Conditions for the Wave Equation," *Mathematics of Computation*, Vol. 49, No. 179, 1987, pp. 65–90.

[10]Thompson, K. W., "Time Dependant Boundary Conditions for Hyperbolic Systems," *Journal of Computational Physics*, Vol. 68, No. 1, 1987, pp. 1–24.

[11]Gustaffson, B., "Far-Field Boundary Conditions for Time-Dependant Hyperbolic Systems," *SIAM Journal on Scientific and Statistical Computing*, Vol. 9, No. 5, 1988, pp. 812–828.

[12]Giles, M. B., "Non-Reflecting Boundary Conditions for Euler Equation Calculations," *AIAA Journal*, Vol. 28, No. 12, 1990, pp. 2050–2058.

[13]Giles, M. B., "Non-Reflecting Boundary Conditions for Euler Equations," Massachusetts Inst. of Technology, Dept. of Aeronautics and Astronautics, TR CFDL-TR-88-1, Cambridge, MA, Feb. 1988.

[14]Kreiss, H. O., "Initial Boundary Value Problems for Hyperbolic Systems," *Communications on Pure and Applied Mathematics*, Vol. 23, No. 3, 1970, pp. 277–298.

[15]Trefethen, L. N., "Group Velocity in Finite Difference Schemes," *SIAM Review*, Vol. 24, No. 2, 1982, pp. 113–136.

[16]Poinsot, T. J., and Lele, S. K., "Boundary Conditions for Direct Simulations of Compressible Viscous Reacting Flows," *Journal of Computational Physics*, Vol. 101, No. 1, 1992, pp. 104–129.

[17]Rudy, D. H., and Strikwerda, J. C., "A Nonreflecting Outflow Boundary Condition for Subsonic Navier-Stokes Calculations," *Journal of Computational Physics*, Vol. 36, No. 1, 1980, pp. 55–70.

[18]Colonius, T., Lele, S. K., and Moin, P., "The Free Compressible Viscous Vortex," *Journal of Fluid Mechanics*, Vol. 230, Sept. 1991, pp. 45–73.

[19]Rai, M. M., and Moin, P., "Direct Numerical Simulation of Transition and Turbulence in a Spatially Evolving Boundary Layer," AIAA Paper 91-1607, June 1991.

[20]Sandham, N. D., and Reynolds, W. C., "A Numerical Investigation of the Compressible Mixing Layer," Stanford Univ., Thermosciences Div., Dept. of Mechanical Engineering, Rept. TF-45, Stanford, CA, Sept. 1989.

[21]Buell, J., and Huerre, P., "Inflow/Outflow Boundary Conditions and Global Dynamics of Spatial Mixing Layers," *Proceedings of the 1988 Summer Program*, Center for Turbulence Research, Stanford Univ., Rept. CTR-S88, Stanford, CA, 1988, pp. 19–27.

[22]Vichnevetsky, R., and Pariser, E. C., "Nonreflecting Upwind Boundaries for Hyperbolic Equations," *Numerical Methods for Partial Differential Equations*, Vol. 2, No. 1, 1986, pp. 1–12.

[23]Vichnevetsky, R., "Invariance Theorems Concerning Reflection at Numerical Boundaries," *Journal of Computational Physics*, Vol. 63, No. 2, 1986, pp. 268–282.